

# AERR-Nav: Adaptive Exploration-Recovery-Reminiscing Strategy for Zero-Shot Object Navigation

Jingzhi Huang<sup>1</sup>, Junkai Huang<sup>2</sup>, Haoyang Yang<sup>1</sup>, Haoang Li<sup>3</sup>, and Yi Wang<sup>1</sup>

<sup>1</sup> Hong Kong Polytechnic University  
jingzhi.huang@connect.polyu.hk

<sup>2</sup> Institute of automation, Chinese Academy of Sciences

<sup>3</sup> Hong Kong University of Science and Technology (Guangzhou)  
<https://github.com/kim-os/AERR-Nav>

**Abstract.** Zero-Shot Object Navigation (ZSON) in unknown multi-floor environments presents a significant challenge. Recent methods, mostly based on semantic value greedy waypoint selection, spatial topology-enhanced memory, and Multimodal Large Language Model (MLLM) as a decision-making framework, have led to improvements. However, these architectures struggle to balance exploration and exploitation for ZSON when encountering unseen environments, especially in multi-floor settings, such as robots getting stuck at narrow intersections, endlessly wandering, or failing to find stair entrances. To overcome these challenges, we propose AERR-Nav, a Zero-Shot Object Navigation framework that dynamically adjusts its state based on the robot’s environment. Specifically, AERR-Nav has the following two key advantages: (1) An Adaptive Exploration-Recovery-Reminiscing Strategy, enables robots to dynamically transition between three states, facilitating specialized responses to diverse navigation scenarios. (2) An Adaptive Exploration State featuring Fast and Slow-Thinking modes helps robots better balance exploration, exploitation, and higher-level reasoning based on evolving environmental information. Extensive experiments on the HM3D and MP3D benchmarks demonstrate that our AERR-Nav achieves state-of-the-art performance among zero-shot methods. Comprehensive ablation studies further validate the efficacy of our proposed strategy and modules.

**Keywords:** Adaptive Exploration-Recovery-Reminiscing Strategy · Adaptive Exploration State · Zero-Shot Object Navigation

## 1 Introduction

Zero-Shot Object Navigation (ZSON) is a fundamental and challenging task in Embodied AI, requiring agents to locate specific objects in an unknown, complex environment based on a natural language description of the target category and visual information [1]. Compared to conventional data-driven learning methods [5, 6, 10, 29, 32, 33, 39], the zero-shot paradigm [2, 7, 13, 16, 34, 41, 49] can adapt to

unseen environments without the need for additional training data. In practical scenarios, for example the open-world environments, this capability allows robots to navigate a completely new environment to retrieve specific items (e.g., a book) for patients. Furthermore, from the perspective of real-world deployment, ZSON methods enable scalable and efficient application across a wide range of diverse domains, as they eliminate the need for environment-specific training, extensive data collection, or task-specific fine-tuning.

Early ZSON methods are primarily designed for single-floor environments. Initially, [9, 23] leveraged Vision-Language Model (VLM) to extract semantic features from RGB observations, which were then integrated with exploration strategies to accomplish object-goal navigation tasks. However, these approaches proved highly inefficient. With the rapid advancement of Multimodal Large Language Model (MLLM), recent works seek to leverage the powerful reasoning capabilities of MLLM to improve navigation efficiency. Consequently, MLLM are frequently employed to select waypoints based on current RGB image [12, 21, 46], value map [14, 16]. Nevertheless, these methods struggle to generalize to multi-floor navigation tasks. As the scale of the environment expands, the demands on the agent for complex geometric perception and path planning increase significantly.

Recent ZSON studies recognize this limitation and propose solutions for navigating across multiple floors. Spatially, methods such as [35, 42, 47] utilize 3D Simultaneous Localization and Mapping (SLAM) to build maps and [22, 37, 43] construct hierarchical topology maps from floors to rooms. To improve efficiency, approaches like [11] prioritize searching nearest frontiers and rely on MLLM for distant planning. Additionally, methods like [19, 50] focus on finding the shortest exploration paths, method [3] further decomposes the exploration state to emulate human cognition, it does so at the cost of making each decision step heavily dependent on an MLLM, leading to substantial token consumption. Despite improving object-finding success rates by enhancing spatial representations and boosting exploration efficiency, these works overlook two critical issues. First, their frameworks lack a well-defined state representation and state transitions; they often overemphasize exploration, leaving robots less robust during navigation and unable to cope effectively with abnormal situation. For example, the robot may fail to locate the entrance to a staircase or get stuck while attempting to reach a frontier point. Second, their exploration strategies fail to adequately adapt to environmental variations in exploration coverage, semantic cues, and structural information and so on, making it difficult to balance exploration, exploitation, and high-level planning.

To enable the robot to simulate human-like thinking and problem-solving approaches, we propose AERR-Nav, In summary, the contributions of our method are as follows: (1) We propose an Adaptive Exploration-Recovery-Reminiscing Strategy that explicitly accounts for the diverse situations a robot may encounter during object search, and better adapts to navigation tasks by dynamically switching among these states. (2) We propose an Adaptive Exploration state featuring Fast and Slow-Thinking modes. The Fast-Thinking mode explic-

itly incorporates priors on the environment’s semantic value and uncertainty estimation to guide efficient exploration, while the Slow-Thinking mode integrates commonsense knowledge with current observations to perform high-level planning. This state helps robots better balance exploration, exploitation, and higher-level reasoning during the task. (3) We achieves state-of-the-art zero-shot performance for ZS-OGN benchmarks, improving SR by 6.9% and SPL by 2.1% on HM3D [28], and SR by 3.4% on MP3D [4]. Ablation studies and comparative experiments further demonstrate the effectiveness of the strategy and modules.

## 2 Related Works

**Object Navigation.** Object navigation refers to the task of guiding a robot to search for a given target object within an unknown environment. The dominant strategies can generally be divided into two primary categories: the first group includes training-dependent methods, such as reinforcement learning and imitation learning, which necessitate extensive training using task-specific datasets [8, 24, 29, 30, 36]. The second category includes zero-shot methods [2, 7, 13, 16, 34, 41, 49], which leverage pre-trained models like VLM [17, 27] or MLLM to enable the robot to exhibit strong adaptability in unseen environments. These methods commonly utilize MLLM as decision-maker. However, they often neglect to consider the robot’s state. Therefore, our zero-shot approach incorporates an MLLM role-playing strategy, allowing the robot to take different actions depending on its current state, thus improving the decision-making process in dynamic and varied contexts.

**Exploration Strategy for Zero-Shot Object Navigation.** Under a strict step budget, balancing exploration and exploitation in complex multi-floor environments is crucial for robots. Most early methods rely heavily on greedy strategies. SSR-ZS [25] constructs semantic maps and utilizes MLLM to identify and select target-relevant frontiers; VLFM [38] employs VLM to build value maps linking frontiers to the target; and SGNavi [37] leverages 3D scene graphs to prompt MLLM for spatial reasoning. However, strategies that depend so heavily on semantic or MLLM-derived scoring often suffer from inefficient exploration. Subsequent approaches have sought to address this limitation. ApexNav [44] introduces an adaptive exploration method that dynamically switches operational modes based on the strength of semantic cues. However, the lack of continuous MLLM reasoning during the exploration process often leads the robot to overlook areas where the target is hidden, particularly when the semantic cues are weak. Similarly, while ASC [11] proposes a coarse-to-fine exploration strategy that combines nearest-frontier exploration with MLLM guidance, it fails to adapt dynamically to environmental variations, causing the robot to simply navigate to the nearest frontier most of the time. In short, we should use the MLLM in moderation and integrate it into the exploration strategy. So, we propose an environment-adaptive exploration state integrated with a fast-and-slow thinking mechanism.

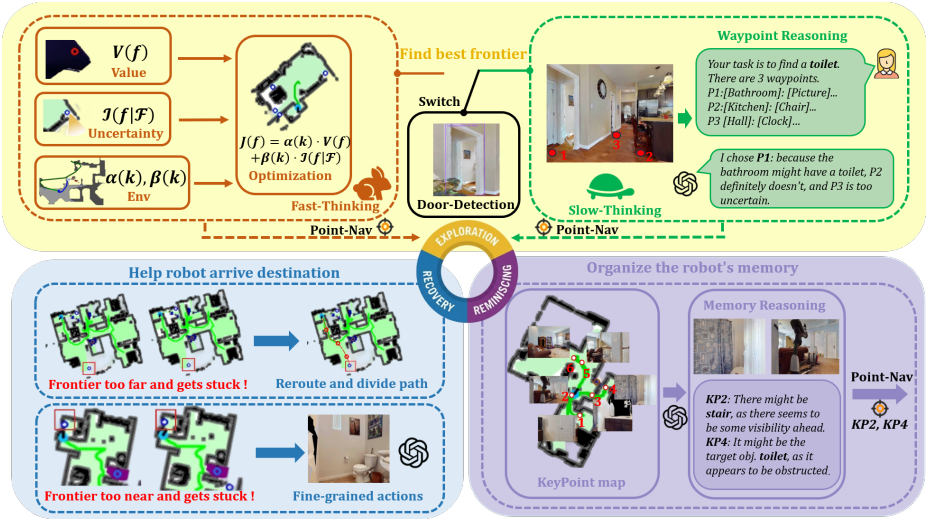


**Fig. 1:** AERR-Nav pipeline: Robot adopts different strategies in different states. During exploration, the optimization function operates as the cerebellum to execute “fast thinking”, while the MLLM serves as the brain to engage in “slow thinking”. When entrapment occurs, two distinct recovery methods are employed depending on the distance to the target frontier point. After completing the exploration of a single floor, MLLM uses keypoint map to guide robot in autonomously revisiting potential target or stairway entrance.

## 3 Method

### 3.1 Task Definition

We formulate ZSON task, the robot needs to locate target objects in unfamiliar environments it has never encountered before. The target object  $c$  is provided as a free-form linguistic description. At each discrete time step  $t$ , the agent perceives the environment through an RGB-D sensor. Concurrently, the agent tracks its relative state  $s_t = (x_t, r_t)$  via on-board odometry, representing its position  $x_t \in \mathbb{R}^3$  and orientation  $r_t \in SO(3)$ . The agent’s decision-making framework must select a discrete action  $a_t$  from the action space  $\mathcal{A} = \{\text{MOVE\_FORWARD}, \text{TURN\_LEFT}, \text{TURN\_RIGHT}, \text{LOOK\_UP}, \text{LOOK\_DOWN}, \text{STOP}\}$ . The locomotion is executed in fixed increments (e.g., 0.25m for translation and  $30^\circ$  for rotation). An episode is deemed a success if the agent issues a STOP command within a proximity threshold of 0.1m from the target object, without exceeding a maximum budget of 500 steps.

### 3.2 Framework Overview

As illustrated in Fig. 1, AERR-Nav is a zero-shot object navigation framework based on Adaptive Exploration-Recovery-Reminiscing Strategy. The robot gen-

erates maps during the navigation based on environmental observations to establish persistent memory, as described in Sec. 3.3, which serves as the foundation for various states. As the robot interacts with the environment, it contains three states that can be switched between as the environment changes: (1) An exploration state with fast and slow thinking, adaptable to the environment, designed to balance exploration and exploitation, as described in Sec. 3.5. (2) A dual recovery state based on the distance of frontier point, used to recover from wandering or getting stuck, as outlined in Sec. 3.6. (3) A reminiscing state based on KeyPoint Map, employed to locate hidden stair entrance and check for possibly missed target object, as discussed in Sec. 3.7. The detailed state transition conditions can be found in Sec. 3.4.

### 3.3 Map Representation

**Visibility Map**  $\mathcal{M}_{\text{vis}}$ . We maintain a 2D occupancy grid map by projecting depth observations into 3D point cloud and subsequently performing Bird’s Eye View (BEV) projection. Based on the boundaries between explored free space and unexplored regions, we extract a set of candidate frontiers  $\mathcal{F} = \{f_1, f_2, \dots, f_n\}$ . These frontiers are categorized into two subsets: intra-floor frontiers  $\mathcal{F}_{\text{floor}}$  and staircase frontiers  $\mathcal{F}_{\text{stair}}$ , where staircases are treated as traversable transitions. The specific geometry-based staircase detection and frontier generation logic follow the [11].

**Exploration Value Map**  $\mathcal{M}_{\text{val}}$ . We define a value function  $V(f)$  for each frontier  $f \in \mathcal{F}_{\text{floor}}$  as follows:

$$V(f) = \alpha \cdot S_{\text{sem}}(f) + \beta \cdot S_{\text{dist}}(f), \quad (1)$$

where the  $S_{\text{sem}}(f)$  evaluates the semantic relevance of a frontier. Using the BLIP-2 [17], we can calculate the score by measuring the cosine similarity between an RGB observation  $I_f$  at the frontier and a set of context-aware text prompts  $T$  (e.g., bathtub or sink when the target is toilet) generated by the MLLM’s common-sense reasoning.  $S_{\text{dist}}(f)$  favors proximal exploration by employing a linear decay function based on the geodesic distance  $d(r, f)$  between the robot’s current position  $r$  and the frontier  $f$ :

$$S_{\text{dist}}(f) = \max\left(0, 1 - \frac{d(r, f)}{d_{\text{max}}}\right), \quad (2)$$

where  $d_{\text{max}}$  represents a predefined normalization constant.

**KeyPoint Map**  $\mathcal{M}_{\text{key}}$ . Inspired by the keyframes of Orb-SLAM2 [26], the difference is that these keyframes are fixed onto a 2D map as keypoints. The criteria for selecting keypoints are as follows: all room entrances and frontiers with open visibility. Frontiers with open visibility can be quantified by the area of the robot’s field of view (FOV) at that point, which is not obstructed by obstacles.

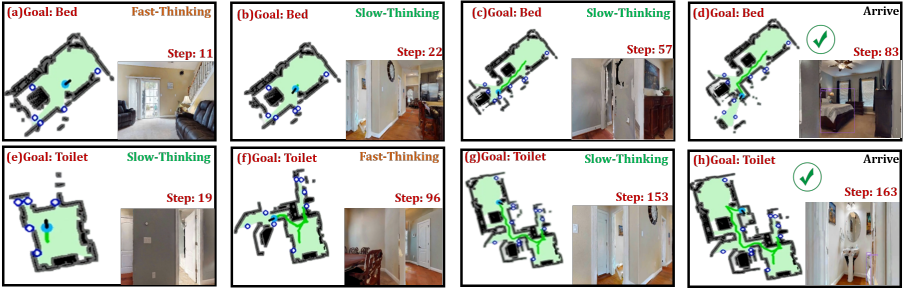


**Fig. 2:** Analysis of examples of exploration strategy: In Example 1, (a) it believes the region behind it has higher value scores and greater uncertainty; (b) after seeing a door, MLLM reasons that a bed is unlikely to be in a bathroom and therefore chooses the hallway; (c) after a period of rapid exploration, it encounters another door and MLLM infers that the bed is more likely to be in a bedroom than in the dining area; and (d) it eventually finds the target bed. In Example 2, (e) upon seeing a door, MLLM judges that the right-side door appears to lead to a bathroom and is thus more likely to contain a toilet; (f) in the area near the right-side door, it does not observe a toilet; fast thinking is triggered and, based on uncertainty, it goes to the left-side region; (g) after a period of fast thinking, the robot originally intended to return to the initial right-side area, but upon seeing a door, MLLM infers that the narrow room may be a bathroom; and (h) it finds the target toilet.

We independently maintain these three distinct map layers for each floor, resulting in a global environmental representation structured as a set of floor-specific tuples:  $\mathcal{M} = \{\langle F_i, \mathcal{M}_{\text{vis}(i)}, \mathcal{M}_{\text{val}(i)}, \mathcal{M}_{\text{key}(i)} \rangle\}_{i=1}^n$ , where  $F_i$  denotes the  $i$ -th floor index.

### 3.4 State Detection and Switching

We use a state machine to describe the robot’s states  $S = \{S_{\text{exp}}, S_{\text{rec}}, S_{\text{rem}}\}$ .  $S_{\text{exp}}$ , which is the robot’s initial state, is triggered when frontier points still exist in the current map.  $S_{\text{rec}}$  is triggered when the distance between the average position of the last  $N_{\text{rec}}$  steps and the position of the  $SN_{\text{rec}}$  last step is less than  $D_{\text{rec}}$  meters. After recovery, the robot switches back to the  $S_{\text{exp}}$ .  $S_{\text{rem}}$  is triggered when there are no new frontier point in the current floor.

### 3.5 Adaptive Exploration State

The switch between fast and slow-thinking occurs based on specific triggers. Doorframes act as connectors between rooms and corridors. When multiple connected regions are available, MLLM may infer that the target object is hidden in a particular region. Therefore, the doorframe detector activates the transition between fast and slow-thinking. Fig. 2 shows how fast and slow-thinking work together to locate objects.

**Fast-Thinking Mode.** We formulate the frontier selection as an optimization problem that balances current values priors with the expected reduction in environmental uncertainty. Let  $\mathcal{Z}_k$  be the observations up to step  $k$ , and  $\rho_{k|k} = p(\Theta|\mathcal{Z}_k)$  denote the current belief of the target  $\Theta$ . When the robot evaluates a candidate frontier  $f \in \mathcal{F}_{\text{floor}}$ , it anticipates a future belief  $\hat{\rho}_{k+1|k} = p(\Theta|\mathcal{Z}_k, \hat{z}_{k+1}) = \mathcal{I}(f|\mathcal{F})$ , where  $\hat{z}_{k+1}$  is a virtual estimate within the FOV at  $f$ :

$$J(f) = \alpha(k) \cdot V(f) + \beta(k) \cdot \mathcal{I}(f|\mathcal{F}), \quad (3)$$

where  $\alpha(k)$  and  $\beta(k)$  are factors that change with the environment, and will be explained later,  $V(f)$  is the prior value (Eq. 1), and  $\mathcal{I}(f|\mathcal{F})$  quantifies the expected uncertainty reduction. To compute this, we first project the FOV at  $f$  to obtain the coverage area  $S_1$ . For the set of semantic scores  $\mathcal{C}$  at the boundaries of  $S_1$ , we apply a Gaussian kernel  $G(\cdot)$  to estimate the spatial information density  $d(\mathbf{p}) = G(\mathcal{C})$ . To account for the redundancy and overlap between multiple frontiers, the total estimated uncertainty  $f_{1-u}$  for a frontier is adjusted by considering the mutual information between overlapping coverage areas. Specifically, the integrated uncertainty at  $f$  is formulated as:

$$\mathcal{I}(f|\mathcal{F}) = \int_{S_1(f)} d(\mathbf{p})d\mathbf{p} + \sum_{f_j \in \mathcal{F}, j \neq f} \text{Area}(S_1(f) \cap S_1(f_j)), \quad (4)$$

where  $\text{Area}(S_1(f) \cap S_1(f_j))$  represents the spatial overlap between the estimated coverage of frontier  $f$  and its neighbors  $f_j$ , more details can be found in the supplementary materials.

$\alpha(k)$  and  $\beta(k)$  are adapted based on the Exploration Reward (ER), which characterizes the robot’s exploration progress and the remaining environmental potential at time  $k$ . The exploration reward  $\text{ER}(k)$  is defined as a multi-factor metric:

$$\text{ER}(k) = \sigma_1 \cdot \frac{|U(k)|}{|E|} + \sigma_2 \cdot \frac{N_{\text{frontier}}(k)}{N_{\text{total}}} + \sigma_3 \cdot \left(1 - \frac{k}{K_{\text{max}}}\right), \quad (5)$$

where  $|U(k)|/|E|$  represents the ratio of the unexplored area to the total environment size at step  $k$ ,  $N_{\text{frontier}}(k)/N_{\text{total}}$  denotes the current density of discovered frontiers, and the final term introduces a temporal decay to prioritize rapid exploration in the early stages of the mission. The state-dependent coefficients  $\alpha(k)$  and  $\beta(k)$  are updated as follows:

$$\beta(k) = \beta_{\text{max}} \cdot \text{ER}(k), \quad \alpha(k) = \alpha_{\text{min}} \cdot (1 - \text{ER}(k)). \quad (6)$$

This formulation ensures a principled transition in the robot’s behavior: during the initial stages or when facing vast unknown regions, the system prioritizes uncertainty reduction through a larger  $\beta(k)$ . As the environment becomes progressively mapped and the step count approaches the limit  $K_{\text{max}}$ , the strategy shifts toward value exploitation via  $\alpha(k)$ .

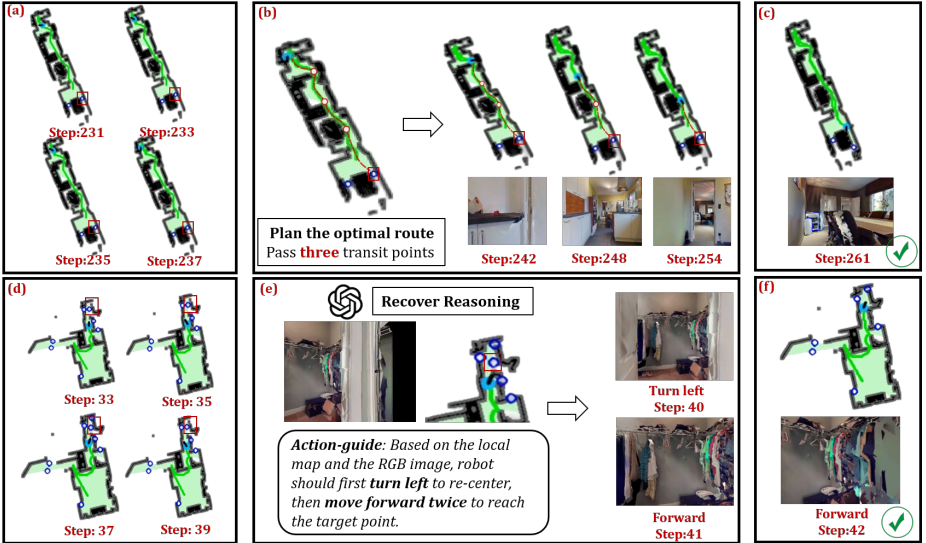


**Fig. 3:** Explanation of the recovery state workflow: (a) and (d) illustrate abnormal behaviors caused by frontier points distance. (b)→(c) demonstrate how to handle overly distant frontier points using a segmented method. (e)→(f) show how MLLM progressively approaches the target frontier point via fine-grained action adjustments.

**Slow-Thinking Mode.** A local room and object topology map is first constructed to enhance the accuracy of MLLM predictions. First, the current RGB image is divided based on the regions of doorframes. Then, each RGB image is processed using RAM [45] to classify the object categories, and Place365 [48] is used to identify the room types, ultimately generating descriptions for different rooms. Following this, prompts are designed to allow MLLM to evaluate, in conjunction with the visibility map and the current RGB image, whether a frontier point is suitable for exploration.

### 3.6 Recovery State

After identifying the frontier point, a pre-trained PointNav strategy is employed, which operates without reliance on a global map. This approach not only reduces computational costs but also enhances operational speed, a method commonly used in many ZSON-based approaches for controlling robot movement. However, practical testing revealed that the robot encounters stagnation when navigating to frontier point that are either too close or too far, causing the robot to move back and forth without reaching the target. To address this practical issue, a dual recovery state is proposed.

As shown in Fig. 3(b), when dealing with distant frontier point, the A\* algorithm is first applied on the 2D visibility map to compute a collision-free path from the current position to the target. By employing an interval sampling



**Fig. 4:** Explanation of how the reminiscing state facilitates progress in task: (a) visualizes the representation of the KeyPoint Map. (b) illustrates how the MLLM chose to keypoints and locate the staircase entrance. (c) shows the robot descending the stairs after locating the stairway entrance and then continuing to find the target.

method, several intermediate points are generated along the path. The target, therefore, becomes to traverse all the intermediate points, and after testing, the robot successfully resumes normal movement.

As shown in Fig. 3(e), when handling nearby frontier points, MLLM is used to generate fine-grained action commands by integrating the RGB image and the local map.

### 3.7 Reminiscing State

Following the completion of single-floor exploration, a two-stage reminiscing process is initiated to ensure thoroughness and facilitate multi-floor transitions. This process relies on  $\mathcal{M}_{\text{key}}$ , where each point preserves a corresponding RGB observation on the global map. This integration allows the MLLM to perform joint spatial-semantic reasoning by synthesizing the global geometric structure with localized visual data. As shown in Fig. 3, the reminiscing logic is executed in two hierarchical stages:

**Target Verification.** The MLLM first reviews the aggregate keypoint collection to identify potential nodes where the target object may have been overlooked. Upon selecting candidate keypoints, the system extracts the RGB images for a secondary, fine-grained confirmation. If verified, the robot navigates to the specific coordinates and executes a terminal approach to the target.

**Look for Staircase.** If no potential target locations are identified, the MLLM shifts focus to detecting potential staircase entrances to enable vertical mobility. The robot employs the PointNav policy to navigate toward the keypoint with the highest probability of containing a staircase. Final alignment with the staircase entrance is achieved through MLLM-guided fine-grained action.

## 4 Experimental Results

In this section, we provide a thorough experimental analysis to validate the our **AERR-Nav** framework. The evaluation is structured to address three fundamental questions: 1. How does our approach perform relative to existing methods? 2. What is the contribution of each individual module to overall performance? 3. Are there any case studies comparing with other methods to highlight the effectiveness of this framework?

### 4.1 Experimental Setup

**Datasets.** We utilize the HM3D [28] and MP3D [4] datasets under the standard Object Goal Navigation (OGN) benchmark. The HM3D validation split consists of 2000 episodes across 20 scenes, encompassing 6 object categories. Similarly, the MP3D validation set contains 2195 episodes spanning 11 scenes and 21 categories. Notably, a statistical analysis of these environments reveals a strong prevalence of multi-story layouts: approximately 65% of the scenes in HM3D and 73% in MP3D feature multiple floors.

**Evaluation Metrics.** To comprehensively evaluate all methods, we employ two standard metrics: Success Rate (SR) and Success weighted by inverse Path Length (SPL). While SR captures the binary outcome of task completion, SPL quantifies the agent’s navigational efficiency by comparing its trajectory against the shortest optimal path, assigning a score of zero to unsuccessful episodes.

**Implementation Details.** We employ RAM [45] to generate category prompts, while Grounding-DINO [20] is utilized for open-vocabulary detection. Object contours are extracted via SAM [15] segmentation. To facilitate boundary reasoning, we leverage BLIP-2 [17] for semantic similarity representation, Places365 [48] for scene classification, and GPT-4o for LLM-based inference. All experiments were conducted online using a single NVIDIA RTX 4090 GPU.

### 4.2 Comparison with SOTA

As shown in Tab. 1, we evaluate our proposed AERR-Nav methods on the HM3D and MP3D datasets. Our method consistently outperforms all existing baselines, establishing a new SOTA performance across both benchmarks in zero-shot settings.

Specifically, on the HM3D dataset, AERR-Nav achieves an impressive 72.3% in SR and 35.6% in SPL. This represents a significant absolute improvement of +6.9% in SR and +2.1% in SPL over the previously best-performing method, ASCENT. Furthermore, on the MP3D dataset, our approach reaches 47.9% SR and 18.7% SPL. Compared to the strong baseline ASCENT, we observe a +3.4% increase in SR. Additionally, AERR-Nav surpasses BeliefMapNav, the prior best in path efficiency on MP3D, yielding a +1.1% gain in SPL.

**Table 1:** Comparison of AERR-Nav and other zero-shot methods on the HM3D and MP3D datasets.

Method	Venue	Zero-shot	HM3D		MP3D	
			SR $\uparrow$	SPL $\uparrow$	SR $\uparrow$	SPL $\uparrow$
ZSON [23]	NeurIPS'22	✓	25.5	12.6	15.3	4.8
ESC [49]	ICML'23	✓	39.2	22.3	28.7	14.2
L3MVN [40]	IROS'23	✓	50.4	23.1	34.9	14.5
PSL [31]	ECCV'24	✓	42.4	19.2	18.9	6.9
VLFM [38]	ICRA'24	✓	52.5	30.4	36.4	17.5
OpenFMNav [16]	NAACL'24	✓	52.5	24.1	37.2	15.7
SG-NAV [37]	NeurIPS'24	✓	54.0	24.9	40.2	16.0
BeliefMapNav [50]	NeurIPS'25	✓	61.4	30.6	37.3	17.6
ASCENT [11]	RAL'26	✓	65.4	33.5	44.5	15.5
<b>AERR-Nav</b>	<b>ours</b>	✓	<b>72.3</b>	<b>35.6</b>	<b>47.9</b>	<b>18.7</b>

To validate cross-floor capabilities, we divide the HM3D episodes into intra-floor (The target object and the robot are initialized on the same floor) and inter-floor (The target object and the robot are initialized on the different floor) scenarios. As shown in Tab. 2, AERR-Nav’s overall enhancement is predominantly driven by its inter-floor breakthrough. Alongside steady intra-floor improvements, our method achieves remarkable cross-level gains, outperforming the strongest baseline, ASCENT, by +29.2% in SR and +12.4% in SPL.

Finally, We attribute these substantial gains to two key factors. First, AERR-Nav employs an optimized strategy that balances the exploration-exploitation trade-off within a limited step budget, maximizing search efficiency. Second, AERR-Nav handles the anomalous behaviors encountered by the robot, saving many cases that would have failed due to such anomalies.

**Table 2:** Performance comparison between intra and inter-floor navigation scenarios.

Method	Intra-Floor Scenarios		Inter-Floor Scenarios		All Episodes	
	SR $\uparrow$	SPL $\uparrow$	SR $\uparrow$	SPL $\uparrow$	SR $\uparrow$	SPL $\uparrow$
VLFM [38]	64.6	37.3	0.4	0.1	52.8	30.5
MFNP [43]	68.4	30.5	13.4	9.8	58.3	26.7
ASCENT [11]	72.6	37.7	33.3	14.9	65.4	33.5
<b>AERR-Nav</b>	<b>75.8</b>	<b>38.1</b>	<b>62.5</b>	<b>27.3</b>	<b>72.3</b>	<b>35.6</b>

### 4.3 Ablative Study

To comprehensively validate the efficacy of the proposed components in AERR-Nav, we conduct extensive ablation study.

**Effectiveness of Different strategy Combinations.** As shown in Tab. 3, the baseline, relying solely on the core exploration strategy, achieves 68.9% and 45.1% SR on HM3D and MP3D, respectively. Integrating the recovery strategy (REC) yields a consistent +1.2% SR increase across both datasets, proving its ability to robustly rescue the agent from physical entrapments. Alternatively, the reminiscing strategy (REM) boosts SR by +1.6% on HM3D and +0.8% on MP3D, demonstrating its effectiveness in using keypoint memory to locate staircases and prevent target omission. Ultimately, the complete AERR-Nav framework (EXP+REC+REM) achieves the highest overall performance. It demonstrates a strong synergy between exploration, recovery, and reminiscing strategy for robust multi-level navigation.

**Effectiveness of Adaptive Exploration State.** We tested the performance of different exploration strategies by modifying the values of  $\alpha$  and  $\beta$  in Eq. 3 and controlling the participation of MLLM. As shown in Tab. 4, relying solely on either semantic information (a) or uncertainty (b) achieves poor navigation performance. While combining these two strategies with fixed weights (c) leads to noticeable improvements, indicating that semantic priors and exploration uncertainty are complementary. The static approach still lacks the flexibility to handle complex environments. By introducing dynamic weighting (e), the performance is further improved. Furthermore, the MLLM consistently enhances navigation efficiency across all configurations. Comparing (c) to (d) and (e) to (f), MLLM’s high-level reasoning provides clear performance gains because it can infer the areas where the target may exist through visual reasoning, rather than relying solely on the calculation results of the optimization function for exploration.

**Effectiveness of VLM and MLLM.** As shown in Tab. 5, using Gemini results in a baseline SR of 70.8% and SPL of 33.8%. The Qwen2.5-VL model performs slightly better, achieving an SR of 71.4% and an SPL of 34.5%. However, GPT-4o demonstrates the highest efficacy. This indicates that GPT-4o provides superior spatial reasoning and zero-shot generalization capabilities. As shown in Tab. 6, CLIP [27] and BLIP-2 [17] achieve comparable performance—yielding SRs of 72.1% and 72.3%, and SPLs of 35.5% and 35.6%, respectively—both of which outperform the BLIP baseline. Notably, BLIP2 maintains a slight edge over CLIP in zero-shot text-to-image retrieval accuracy.

To further demonstrate the effectiveness of our AERR-Nav, we compare it against a strong recent baseline ASCENT [11] on the same navigation episode.

As shown in Fig. 5, our AERR-Nav completes the task with fewer time steps, highlighting the efficiency of our exploration strategy. The underlying reason is as follows. Comparing Fig. 5(c) and Fig. 5(i), the left half of the environment is

**Table 3:** Ablation study of different strategy combinations on the HM3D and MP3D.

#	Strategy Combinations			HM3D		MP3D	
	EXP	REC	REM	SR $\uparrow$	SPL $\uparrow$	SR $\uparrow$	SPL $\uparrow$
1	✓			68.9	34.5	45.1	17.2
2	✓	✓		70.1	35.2	46.3	17.4
3	✓		✓	70.5	34.9	45.9	16.8
4	✓	✓	✓	<b>72.3</b>	<b>35.6</b>	<b>47.9</b>	<b>18.7</b>

**Table 4:** Ablation study of the adaptive exploration strategy. Performance comparison of semantic and uncertainty-based exploration, static versus dynamic weighting, and MLLM integration on the HM3D and MP3D datasets.

Exploration Strategy	MLLM	HM3D		MP3D	
		SR $\uparrow$	SPL $\uparrow$	SR $\uparrow$	SPL $\uparrow$
(a) Semantic ( $\alpha = 1, \beta = 0$ )		67.2	29.3	41.1	14.8
(b) Uncertainty ( $\alpha = 0, \beta = 1$ )		66.8	31.1	41.8	15.5
(c) Semantic + Uncertainty ( $\alpha = 0.5, \beta = 0.5$ )		68.5	33.4	43.3	16.3
(d) Semantic + Uncertainty ( $\alpha = 0.5, \beta = 0.5$ )	✓	69.8	34.2	45.4	17.1
(e) Semantic + Uncertainty (Dynamic $\alpha, \beta$ )		69.3	33.8	45.9	17.3
<b>(f) Semantic + Uncertainty (Dynamic <math>\alpha, \beta</math>)</b>	✓	<b>72.3</b>	<b>35.6</b>	<b>47.9</b>	<b>18.7</b>

dominated by a corridor, whereas the right half mainly contains a bathroom and a dressing room. Our AERR-Nav chooses to explore the hall, while ASCENT explores the bathroom and dressing room, which results in a substantial waste of steps for ASCENT. ASCENT made this choice because its coarse-grained exploration selects the nearest frontier point, in other words, MLLM reasoning is only triggered when no frontier points exist near the robot. In contrast, our AERR-Nav triggers MLLM reasoning upon detecting a door. MLLM infers that sofa is unlikely in dressing room or bathroom, thus guiding the robot to explore the hallway as shown in Fig. 5(d).

As shown in Fig. 6, our AERR-Nav enables the robot to recall and localize the staircase entrance, allowing it to continue and complete the cross-floor task, which demonstrates the importance of the reminiscing strategy. As illustrated in Fig. 6(a), when no other frontier points are available, AERR-Nav enters a recall

**Table 5:** Effect of the MLLM on HM3D.

Model	SR $\uparrow$	SPL $\uparrow$
Gemini	70.8	33.8
Qwen2.5-VL	71.4	34.5
<b>GPT-4o</b>	<b>72.3</b>	<b>35.6</b>

**Table 6:** Effect of the MLLM on HM3D.

Model	SR $\uparrow$	SPL $\uparrow$
Blip [18]	70.9	35.1
Clip [27]	72.1	35.5
<b>Blip-2 [17]</b>	<b>72.3</b>	<b>35.6</b>

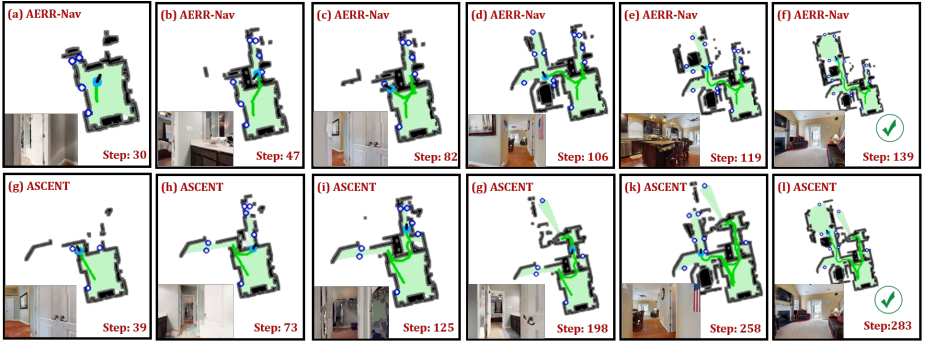


**Fig. 5:** Case Study1: (a)–(f)/(g)–(l) illustrate the complete process of AERR-Nav/ASCENT [11] searching for the sofa.

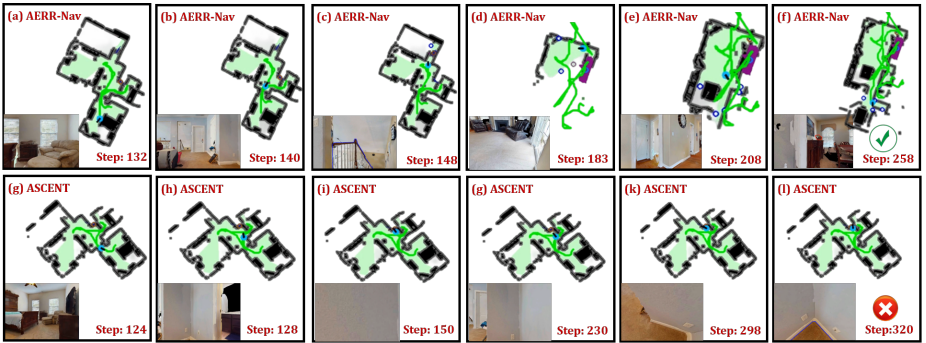


**Fig. 6:** Case Study2: The visualization starts after each method has finished exploring the single-floor. (a)–(f)/(g)–(l) show the process of our AERR-Nav/ASCENT [11] searching for the potted plant.

mode. As shown in Fig. 6(b) and 6(c), the MLLM then guides the agent to hypothesize a likely location of the staircase entrance and successfully discovers the staircase. This ultimately enables the agent to accomplish the cross-floor task. In contrast, ASCENT fails to identify the staircase entrance and keeps wandering repeatedly, resulting in task failure.

## 5 Conclusion

we presented AERR-Nav, a zero-shot object navigation framework for unknown multi-floor environments. To address the limitations of prior methods, we introduces an AERR strategy to effectively handle navigational contingencies. Then, we proposed an Adaptive Exploration state, allowing the agent to dynamically adapt to environments. Extensive experiments on HM3D and MP3D datasets demonstrate the effectiveness of our approach, achieving state-of-the-art performance among zero-shot methods.

## References

1. Batra, D., Gokaslan, A., Kembhavi, A., Maksymets, O., Mottaghi, R., Savva, M., Toshev, A., Wijmans, E.: Objectnav revisited: On evaluation of embodied agents navigating to objects. arXiv preprint [arXiv:2006.13171](https://arxiv.org/abs/2006.13171) (2020)
2. Cai, Y., He, X., Wang, M., Guo, H., Yau, W.Y., Lv, C.: Cl-cotnav: Closed-loop hierarchical chain-of-thought for zero-shot object-goal navigation with vision-language models. arXiv preprint [arXiv:2504.09000](https://arxiv.org/abs/2504.09000) (2025)
3. Cao, Y., Zhang, J., Yu, Z., Liu, S., Qin, Z., Zou, Q., Du, B., Xu, K.: Cognav: Cognitive process modeling for object goal navigation with llms. In: Proceedings of the IEEE/CVF International Conference on Computer Vision (ICCV). pp. 9550–9560 (2025)
4. Chang, A., Dai, A., Funkhouser, T., Halber, M., Niessner, M., Savva, M., Song, S., Zeng, A., Zhang, Y.: Matterport3d: Learning from rgb-d data in indoor environments. arXiv preprint [arXiv:1709.06158](https://arxiv.org/abs/1709.06158) (2017)
5. Chaplot, D.S., Gandhi, D., Gupta, A., Salakhutdinov, R.: Object goal navigation using goal-oriented semantic exploration. In: Advances in Neural Information Processing Systems (NeurIPS) (2020)
6. Chen, S., Chabal, T., Laptev, I., Schmid, C.: Object goal navigation with recursive implicit maps. 2023 IEEE/RSJ International Conference on Intelligent Robots and Systems (IROS) pp. 7089–7096 (2023)
7. Debnath, A., Stein, G.J., Kosecka, J.: Semnav: A model-based planner for zero-shot object goal navigation using vision-foundation models. arXiv preprint [arXiv:2506.03516](https://arxiv.org/abs/2506.03516) (2025)
8. Fukushima, R., Ota, K., Kanezaki, A., Sasaki, Y., Yoshiyasu, Y.: Object memory transformer for object goal navigation. In: 2022 International Conference on Robotics and Automation (ICRA). pp. 11288–11294. IEEE (2022)
9. Gadre, S.Y., Wortsman, M., Ilharco, G., Schmidt, L., Song, S.: Cows on pasture: Baselines and benchmarks for language-driven zero-shot object navigation. In: Proceedings of the IEEE/CVF Conference on Computer Vision and Pattern Recognition (CVPR). pp. 23171–23181 (2023)
10. Ginting, M.F., Kim, S.K., Fan, D.D., Palieri, M., Kochenderfer, M.J., akbar Aghamohammadi, A.: Seek: Semantic reasoning for object goal navigation in real world inspection tasks. In: Proc. of Robotics: Science and Systems (RSS) (2024)
11. Gong, Z., Li, R., Hu, T., Qiu, R., Kong, L., Zhang, L., Zhao, G., Ding, Y., Liang, J.: Stairway to success: An online floor-aware zero-shot object-goal navigation framework via llm-driven coarse-to-fine exploration. IEEE Robotics and Automation Letters (2026)
12. Gu, Z., Zhou, Y., Xue, Y., Wang, H.: Curiosity-driven zero-shot object navigation with vision-language models. IEEE Robotics and Automation Letters (2026)
13. Guan, T., Yang, Y., Cheng, H., Lin, M., Kim, R., Madhivanan, R., Sen, A., Manocha, D.: Loc-zson: Language-driven object-centric zero-shot object retrieval and navigation. arXiv preprint [arXiv:2405.05363](https://arxiv.org/abs/2405.05363) (2024)
14. Han, P., Zhang, M., Tang, H., ZHENG, Y., et al.: Hule-nav: Human-like exploration for zero-shot object navigation via vision-language models. In: NeurIPS 2024 Workshop on Behavioral Machine Learning (2024)
15. Kirillov, A., Mintun, E., Ravi, N., Mao, H., Rolland, C., Gustafson, L., Xiao, T., Whitehead, S., Berg, A.C., Lo, W.Y., et al.: Segment anything. In: Proceedings of the IEEE/CVF International Conference on Computer Vision (ICCV). pp. 4015–4026 (2023)

16. Kuang, Y., Lin, H., Jiang, M.: Openfmnav: Towards open-set zero-shot object navigation via vision-language foundation models. In: Findings of the Association for Computational Linguistics: NAACL 2024. pp. 338–351 (2024)
17. Li, J., Li, D., Savarese, S., Hoi, S.: Blip-2: Bootstrapping language-image pre-training with frozen image encoders and large language models. In: International conference on machine learning. pp. 19730–19742. PMLR (2023)
18. Li, J., Li, D., Xiong, C., Hoi, S.: Blip: Bootstrapping language-image pre-training for unified vision-language understanding and generation. In: International conference on machine learning. pp. 12888–12900. PMLR (2022)
19. Liu, R., Xu, X., Yuan, S., Xie, L.: Handle object navigation as weighted traveling repairman problem. arXiv preprint [arXiv:2503.06937](https://arxiv.org/abs/2503.06937) (2025)
20. Liu, S., Zeng, Z., Ren, T., Li, F., Zhang, H., Yang, J., Jiang, Q., Li, C., Yang, J., Su, H., et al.: Grounding dino: Marrying dino with grounded pre-training for open-set object detection. In: European Conference on Computer Vision (ECCV). pp. 38–55. Springer (2024)
21. Long, Y., Cai, W., Wang, H., Zhan, G., Dong, H.: Instructnav: Zero-shot system for generic instruction navigation in unexplored environment. arXiv preprint [arXiv:2406.04882](https://arxiv.org/abs/2406.04882) (2024)
22. Loo, J., Wu, Z., Hsu, D.: Open scene graphs for open-world object-goal navigation. *The International Journal of Robotics Research* (2025), <https://doi.org/10.1177/02783649251369549>
23. Majumdar, A., Aggarwal, G., Devnani, B., Hoffman, J., Batra, D.: Zson: Zero-shot object-goal navigation using multimodal goal embeddings. *Advances in Neural Information Processing Systems (NeurIPS)* **35**, 32340–32352 (2022)
24. Maksymets, O., Cartillier, V., Gokaslan, A., Wijmans, E., Galuba, W., Lee, S., Batra, D.: Thda: Treasure hunt data augmentation for semantic navigation. In: Proceedings of the IEEE/CVF International Conference on Computer Vision (ICCV). pp. 15374–15383 (2021)
25. Meng, X., Li, D., Mao, Z., Yang, Y., Song, W.: Ssr-zson: Zero-shot object navigation via spatial-semantic relations within a hierarchical exploration framework. arXiv preprint [arXiv:2509.24763](https://arxiv.org/abs/2509.24763) (2025)
26. Mur-Artal, R., Tardós, J.D.: Orb-slam2: An open-source slam system for monocular, stereo, and rgb-d cameras. *IEEE Transactions on Robotics (TRO)* **33**(5), 1255–1262 (2017)
27. Radford, A., Kim, J.W., Hallacy, C., Ramesh, A., Goh, G., Agarwal, S., Sastry, G., Askell, A., Mishkin, P., Clark, J., et al.: Learning transferable visual models from natural language supervision. In: International Conference on Machine Learning (ICML). pp. 8748–8763. PMLR (2021)
28. Ramakrishnan, S.K., Gokaslan, A., Wijmans, E., Maksymets, O., Clegg, A., Turner, J., Undersander, E., Galuba, W., Westbury, A., Chang, A.X., et al.: Habitat-matterport 3d dataset (hm3d): 1000 large-scale 3d environments for embodied ai. arXiv preprint [arXiv:2109.08238](https://arxiv.org/abs/2109.08238) (2021)
29. Ramakrishnan, S.K., Chaplot, D.S., Al-Halah, Z., Malik, J., Grauman, K.: Poni: Potential functions for objectgoal navigation with interaction-free learning. In: Proceedings of the IEEE/CVF Conference on Computer Vision and Pattern Recognition (CVPR). pp. 18890–18900 (2022)
30. Ramrakhya, R., Batra, D., Wijmans, E., Das, A.: Pirlnav: Pretraining with imitation and rl finetuning for objectnav. In: Proceedings of the IEEE/CVF Conference on Computer Vision and Pattern Recognition (CVPR). pp. 17896–17906 (2023)

31. Sun, X., Liu, L., Zhi, H., Qiu, R., Liang, J.: Prioritized semantic learning for zero-shot instance navigation. In: European Conference on Computer Vision (ECCV). pp. 161–178. Springer (2024)
32. Wang, H., Sun, B., Xing, J., Yang, F., Hutter, M., Shah, D., Scaramuzza, D., Pollefeys, M.: What matters in rl-based methods for object-goal navigation? an empirical study and a unified framework. arXiv preprint [arXiv:2510.01830](https://arxiv.org/abs/2510.01830) (2025)
33. Wasserman, J., Chowdhary, G., Gupta, A., Jain, U.: Exploitation-Guided Exploration for Semantic Embodied Navigation. In: 2024 IEEE International Conference on Robotics and Automation (ICRA). pp. 2901–2908 (2024)
34. Wen, C., Huang, Y., Huang, H., Huang, Y., Yuan, S., Hao, Y., Lin, H., Liu, Y.S., Fang, Y.: Zero-shot object navigation with vision-language models reasoning. In: International Conference on Pattern Recognition (ICPR). pp. 389–404. Springer (2025)
35. Yang, Y., Yang, H., Zhou, J., Chen, P., Zhang, H., Du, Y., Gan, C.: 3d-mem: 3d scene memory for embodied exploration and reasoning. In: Proceedings of the IEEE/CVF Conference on Computer Vision and Pattern Recognition (CVPR). pp. 17294–17303 (2025)
36. Ye, X., Yang, Y.: Efficient robotic object search via hiem: Hierarchical policy learning with intrinsic-extrinsic modeling. IEEE Robotics and Automation Letters **6**(3), 4425–4432 (2021)
37. Yin, H., Xu, X., Wu, Z., Zhou, J., Lu, J.: Sg-nav: Online 3d scene graph prompting for llm-based zero-shot object navigation. Advances in Neural Information Processing Systems (NeurIPS) **37**, 5285–5307 (2024)
38. Yokoyama, N., Ha, S., Batra, D., Wang, J., Bucher, B.: Vlfm: Vision-language frontier maps for zero-shot semantic navigation. In: 2024 IEEE International Conference on Robotics and Automation (ICRA). pp. 42–48. IEEE (2024)
39. Yoo, H., Choi, Y., Park, J., Oh, S.: Commonsense-aware object value graph for object goal navigation. IEEE Robotics and Automation Letters **9**(5), 4423–4430 (2024)
40. Yu, B., Kasaei, H., Cao, M.: L3mvm: Leveraging large language models for visual target navigation. In: 2023 IEEE/RSJ International Conference on Intelligent Robots and Systems (IROS). pp. 3554–3560. IEEE (2023)
41. Yu, B., Liu, Y., Han, L., Kasaei, H., Li, T., Cao, M.: Vln-game: Vision-language equilibrium search for zero-shot semantic navigation. arXiv preprint [arXiv:2411.11609](https://arxiv.org/abs/2411.11609) (2024)
42. Zhang, J., Li, Z., Wang, S., Shi, X., Wei, Z., Wu, Q.: Spatialnav: Leveraging spatial scene graphs for zero-shot vision-and-language navigation. arXiv preprint [arXiv:2601.06806](https://arxiv.org/abs/2601.06806) (2026)
43. Zhang, L., Wang, H., Xiao, E., Zhang, X., Zhang, Q., Jiang, Z., Xu, R.: Multi-floor zero-shot object navigation policy. In: 2025 IEEE International Conference on Robotics and Automation (ICRA). pp. 6416–6422. IEEE (2025)
44. Zhang, M., Du, Y., Wu, C., Zhou, J., Qi, Z., Ma, J., Zhou, B.: Apexnav: An adaptive exploration strategy for zero-shot object navigation with target-centric semantic fusion. IEEE Robotics and Automation Letters (2025)
45. Zhang, Y., Huang, X., Ma, J., Li, Z., Luo, Z., Xie, Y., Qin, Y., Luo, T., Li, Y., Liu, S., et al.: Recognize anything: A strong image tagging model. In: Proceedings of the IEEE/CVF Conference on Computer Vision and Pattern Recognition (CVPR). pp. 1724–1732 (2024)
46. Zhao, X., Cai, W., Tang, L., Wang, T.: Imaginenav: Prompting vision-language models as embodied navigator through scene imagination. arXiv preprint [arXiv:2410.09874](https://arxiv.org/abs/2410.09874) (2024)

47. Zheng, W., Chen, H., Lu, X., Ou, L., Yu, X.: 3dgsnav: Enhancing vision-language model reasoning for object navigation via active 3d gaussian splatting. arXiv preprint [arXiv:2602.12159](https://arxiv.org/abs/2602.12159) (2026)
48. Zhou, B., Lapedriza, A., Khosla, A., Oliva, A., Torralba, A.: Places: A 10 million image database for scene recognition. *IEEE Transactions on Pattern Analysis and Machine Intelligence (TPAMI)* **40**(6), 1452–1464 (2017)
49. Zhou, K., Zheng, K., Pryor, C., Shen, Y., Jin, H., Getoor, L., Wang, X.E.: Esc: Exploration with soft commonsense constraints for zero-shot object navigation. In: *International Conference on Machine Learning (ICML)*. pp. 42829–42842. PMLR (2023)
50. Zhou, Z., Hu, Y., Zhang, L., Li, Z., Chen, S.: Beliefmapnav: 3d voxel-based belief map for zero-shot object navigation. arXiv preprint [arXiv:2506.06487](https://arxiv.org/abs/2506.06487) (2025)